Available online at www.sciencedirect.com
ScienceDirect
Journal of Organometallic Chemistry 692 (2007) 3236–3247
Journal of Organometallic Chemistry
www.elsevier.com/locate/jorganchem

Synthesis and characterization of new paramagnetic tetraaryl derivatives of chromium and molybdenum

Pablo J. Alonso, Juan Forniés, M[a] Angeles García-Monforte, Antonio Martín, Babil Menjón *, Conrado Rillo

Instituto de Ciencia de Materiales de Aragón, Facultad de Ciencias, Universidad de Zaragoza–C.S.I.C., C/ Pedro Cerbuna 12, E-50009 Zaragoza, Spain

Received 24 December 2006; received in revised form 14 March 2007; accepted 14 March 2007
Available online 24 March 2007

Abstract

The low-temperature reaction of $[CrCl_3(thf)_3]$ with $LiC_6H_3Cl_2$-2,6 yields the organochromium(III) compound $[Li(thf)_4][Cr^{III}(C_6H_3Cl_2\text{-}2,6)_4]$ (**1**) in 48% yield. The homoleptic, anionic species $[Cr^{III}(C_6H_3Cl_2\text{-}2,6)_4]^-$ is electrochemically related to the neutral one $[Cr^{IV}(C_6H_3Cl_2\text{-}2,6)_4]$ (**2**) through a reversible one-electron exchange process ($E_{1/2} = 0.16$ V, $\Delta E_p = 0.09$ V, $i_{pa}/i_{pc} = 1.18$). Compound **2** was isolated in 74% yield by chemical oxidation of **1** with $[N(C_6H_4Br\text{-}4)_3][SbCl_6]$. Attempts to prepare the salt $[NBu_4][Cr^{III}(C_6Cl_5)_4]$ (**4**) by direct arylation of $[CrCl_3(thf)_3]$ with LiC_6Cl_5 in the presence of $[NBu_4]Br$ gave the organochromium(II) salt $[NBu_4]_2[Cr^{II}(C_6Cl_5)_4]$ (**3**) instead, as the result of a reduction process. The salt $[NBu_4][Cr^{III}(C_6Cl_5)_4]$ (**4**) was cleanly prepared by comproportionation of **3** and $[Cr^{IV}(C_6Cl_5)_4]$. The reaction of $[MoCl_4(dme)]$ with LiC_6Cl_5 in Et_2O solution proceeded with oxidation of the metal center to give the paramagnetic ($S = 1/2$), five-coordinate salt $[Li(thf)_4][Mo^{V}O(C_6Cl_5)_4]$ (**5**). The crystal and molecular structures of **1** and **2** have been established by X-ray diffraction methods. The magnetic properties of **1** and **4** ($S = 3/2$) as well as those of **2** ($S = 1$) have been established by EPR spectroscopy as well as by ac and dc magnetization measurements.

Keywords: Organochromium; Organomolybdenum; Homoleptic compounds; EPR spectroscopy; Cyclic voltammetry; Electronic exchange

1. Introduction

Homoleptic σ-organochromium(III) derivatives bearing no additional ancillary ligands can be considered still today as rare chemical species [1]. To the best of our knowledge just a few precedents have been isolated for the following stoichiometries: $[Cr^{III}R_3]$ ($R = CH(SiMe_3)_2$ [2]), $[Cr^{III}R_4]^-$ ($R = C_6Cl_5$ [3], $C_6H_2Me_3$-2,4,6 [4], C_6H_4OMe-2 [5]), $[Cr^{III}R_5]^{2-}$ ($R = Ph$ [6,7], C_6F_5 [8]), and $[Cr^{III}R_6]^{3-}$ ($R = Me$ [9], Ph [6,10], C_6H_4Ph–4 [5]). All of these complexes have an open-shell electronic structure [11] and are far from conforming to the 18-electron (or Effective Atomic Number) rule. For the correct characterization of this kind of compounds, EPR spectroscopy is an invaluable tool as it is able to provide direct information on the electronic structure of the unpaired electrons of the d^3 Cr^{III} metal ion. Moreover, given that the spin state is, as a rule, $S = 3/2$, the relevant EPR parameters would be expected to be highly sensitive to small changes in the coordination sphere of the paramagnetic center as has been found in classic coordination chemistry.

Compound $[Li(thf)_4][Cr^{III}(C_6Cl_5)_4]$ was found to exhibit interesting electrochemical behavior, with the following three homoleptic species connected by consecutive one-electron exchange processes: $[Cr^{IV}(C_6Cl_5)_4]/[Cr^{III}(C_6Cl_5)_4]^-/[Cr^{II}(C_6Cl_5)_4]^{2-}$ [3a]. This rich behavior was possible because of the versatility of the C_6Cl_5 group as a ligand, which is able to act as a standard monodentate σ-bonded ligand and also as a poor chelating one by establishing a secondary bonding interaction with the metal center through

* Corresponding author. Tel.: +34 976762293; fax: +34 976761187.
E-mail address: menjon@unizar.es (B. Menjón).

0022-328X/$ - see front matter © 2007 Elsevier B.V. All rights reserved.
doi:10.1016/j.jorganchem.2007.03.028

one of its *ortho*-Cl substituents. We sought to test whether the related $C_6H_3Cl_2$-2,6 group, that also bears *ortho*-Cl substituents but has a markedly different electron-withdrawing character could also exhibit this ability to match the electronic and stereochemical requirements of chromium in different oxidation states. In this paper we describe the synthesis of the new pseudo-octahedral anionic species $[Cr^{III}(C_6H_3Cl_2\text{-}2,6)_4]^-$, and compare its electronic and electrochemical properties with those of the known $[Cr^{III}(C_6Cl_5)_4]^-$ anion. One-electron oxidation of the $[Cr^{III}(C_6H_3Cl_2\text{-}2,6)_4]^-$ anion gave the neutral species $[Cr^{IV}(C_6H_3Cl_2\text{-}2,6)_4]$, which has been structurally characterized. Our attempts to prepare an analogous homoleptic molybdenum derivative gave the five-coordinate oxo species $[Mo^{V}O(C_6Cl_5)_4]^-$ instead, as the result of an oxidation process.

2. Results and discussion

2.1. Synthesis and electrochemical behavior of the homoleptic polychloroarylchromium compounds *1*–*4*

The low-temperature reaction (between −78 and 0 °C) of the halo-complex $[CrCl_3(thf)_3]$ with $LiC_6H_3Cl_2$-2,6 in Et_2O, followed by CH_2Cl_2 extraction and subsequent treatment with thf and Et_2O led to the formation of the organochromium(III) compound $[Li(thf)_4][Cr^{III}(C_6H_3Cl_2\text{-}2,6)_4]$ (**1**), which was isolated as a violet solid in 48% yield (Scheme 1). Compound **1** is highly sensitive to oxygen and moisture and also has a rather limited thermal stability, decomposing readily at room temperature both in solution and in the solid state. With regard to stability and solubility properties, the behavior of **1** is similar to that observed for the analogous pentachlorophenyl derivative $[Li(thf)_4][Cr^{III}(C_6Cl_5)_4]$ [3]. Complex **1**, however, is appreciably less soluble in thf than the corresponding pentachlorophenyl homologous species.

The 2,6-dichlorophenyl-derivative **1** has been characterized by analytical and spectroscopic methods. Characterization of **1** also includes a detailed study of its magnetic properties (see below). The IR spectrum shows well-defined, sharp absorptions, including two strong ones at 887 and 1043 cm^{-1}, which can be assigned to the symmetric and asymmetric vibrations of the C–O–C link within the $[Li(thf)_4]^+$ cation [12]. In the absence of any detailed vibrational study of the 2,6-dichlorophenyl group and derivatives thereof, a reliable assignment of the remaining absorptions in the IR spectrum of **1** cannot be made. The MS (FAB−) of **1** shows the peaks corresponding to the parent anion $[Cr(C_6H_3Cl_2\text{-}2,6)_4]^-$ and to fragments with the formula $[Cr(C_6H_3Cl_2\text{-}2,6)_{4-n}Cl_n]^-$ ($n = 1, 2$), deriving from the stepwise replacement of chlorinated aryl groups by Cl atoms. The isotopic distribution observed for all those peaks is in good agreement with the suggested formulation.

The redox behavior of **1** has been studied by electrochemical methods. The room temperature cyclic voltammogram of **1** in CH_2Cl_2 solution measured between −1.6 and +1.6 V (Fig. 1) shows an oxidation peak, $(E_p)_{ox} = 0.20$ V, which is recovered in the returning scan: $(E_p)_{red} = 0.11$ V. This couple corresponds to an electrochemically

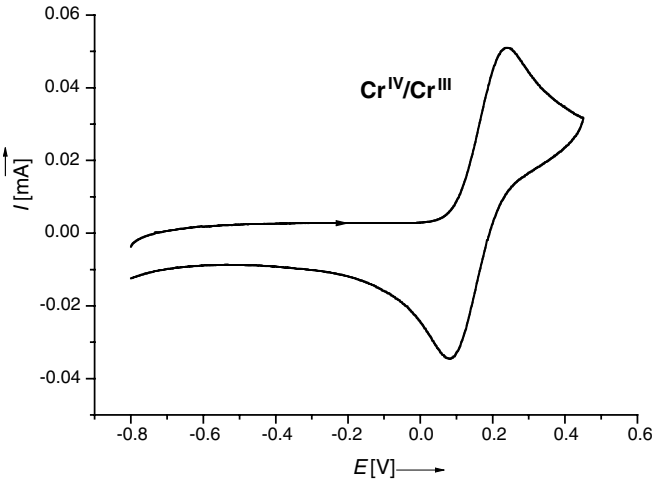

Fig. 1. The CV of **1** in CH_2Cl_2 solution.

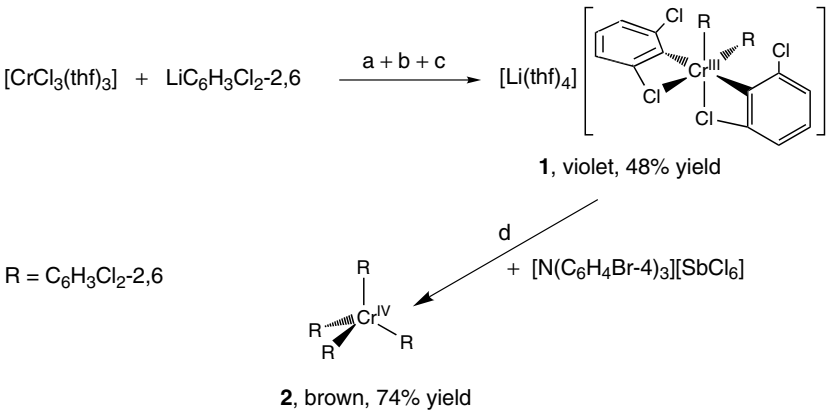

Scheme 1. Experimental procedure to obtain **1** and **2**: (a) reaction in Et_2O at −78 °C; (b) extraction in CH_2Cl_2; (c) addition of thf; (d) in CH_2Cl_2 at 0 °C.

reversible semisystem with $E_{1/2} = 0.16$ V, $\Delta E_p = 0.09$ V and $i_{pa}/i_{pc} = 1.18$. By comparing this behavior with that exhibited by the perchlorinated species $[Li(thf)_4][Cr^{III}(C_6Cl_5)_4]$ [3a], it is apparent that the potential required to oxidize the anionic $[Cr^{III}R_4]^-$ homoleptic species to the corresponding $[Cr^{IV}R_4]$ neutral ones sharply decreases on going from $R = C_6Cl_5$ ($E_{1/2} = 0.76$ V) to $R = C_6H_3Cl_2$-2,6 ($E_{1/2} = 0.16$ V) (*cf.* the vanadium system [13]). An electron exchange process associated with the $[Cr^{III}R_4]^-/[Cr^{II}R_4]^{2-}$ couple—which was detectable for $R = C_6Cl_5$—was not observed for $R = C_6H_3Cl_2$-2,6 in the measured range. Both observations are attributable to the significantly smaller electron-withdrawing ability of the $C_6H_3Cl_2$-2,6 group in comparison with that associated with the perchlorinated one.

The neutral homoleptic species $[Cr^{IV}(C_6H_3Cl_2\text{-}2,6)_4]$ (**2**) was obtained by treatment of **1** with $[N(C_6H_4Br\text{-}4)_3][SbCl_6]$ as the result of a one-electron oxidation process (Scheme 1). Complex **2** was isolated as an analytically pure brown solid in 78% yield. Compared with its perchlorinated homologous species $[Cr^{IV}(C_6Cl_5)_4]$ [3a], complex **2** exhibits a substantially higher thermal stability. This feature, together with the appreciably higher solubility of **2** in the most common organic solvents, enabled us to obtain single crystals suitable for X-ray diffraction purposes and thus to establish its molecular structure (see below).

The electrochemical behavior of **2** in CH_2Cl_2 solution is qualitatively similar to that discussed above for complex **1**. Hence, it can be concluded that **1** and **2** are actually the two chemical species involved in that electrochemical process.

The salt $[NBu_4][Cr^{III}(C_6Cl_5)_4]$ could not be obtained by direct reaction of $[CrCl_3(thf)_3]$ with LiC_6Cl_5 in the presence of $[NBu_4]Br$. Under these conditions, arylation of the metal center takes place together with a formal one-electron reduction process (Scheme 2), eventually yielding $[NBu_4]_2[Cr^{II}(C_6Cl_5)_4]$ (**3**). The targeted organochromate(III) salt $[NBu_4][Cr^{III}(C_6Cl_5)_4]$ (**4**) was eventually obtained in *ca.* 70% yield by a clean comproportionation reaction between the homoleptic organochromium species in the adjacent oxidation states, $[NBu_4]_2[Cr^{II}(C_6Cl_5)_4]$ (**3**) and $[Cr^{IV}(C_6Cl_5)_4]$ (Scheme 2). The $[NBu_4]^+$ cation has in general a better behavior in organometallic and coordination chemistry than the $[Li(thf)_4]^+$ cation, the latter being hygroscopic, prone to undergo dissociation of thf molecules and hence showing a more pronounced electrophilic character. As expected, the salt $[NBu_4][Cr^{III}(C_6Cl_5)_4]$ (**4**) shows an enhanced stability in comparison with the $[Li(thf)_4][Cr^{III}(C_6Cl_5)_4]$ salt. These two salts exhibit the same electrochemical behavior. The EPR spectrum of **4** as well as its magnetic properties will be discussed below.

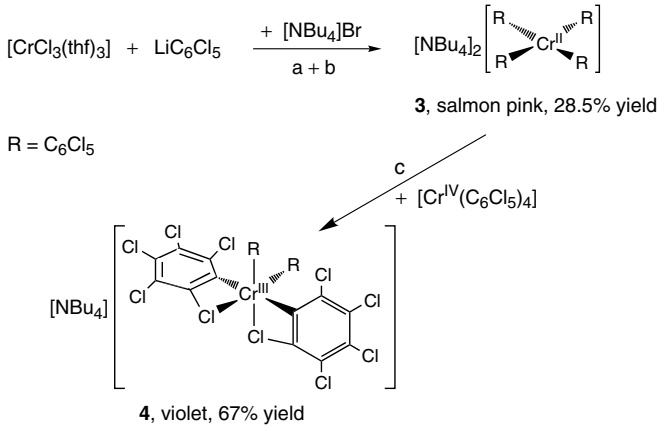

Scheme 2. Experimental procedure to obtain **3** and **4**: (a) reaction in Et_2O at −78 °C; (b) extraction in CH_2Cl_2; (c) in CH_2Cl_2 at 0 °C.

2.2. Structural characterization of the homoleptic polychloroarylchromium compounds *1* and *2*

The crystal and molecular structures of **1** and **2** were determined by X-ray diffraction methods. Crystal data and other details of the structure analyses are presented in Table 1. Crystals of **1** consist of separate $[Li(thf)_4]^+$ cations and $[Cr^{III}(C_6H_3Cl_2\text{-}2,6)_4]^-$ anions with no sign of any kind of covalent interaction between them. The $[Li(thf)_4]^+$ cation shows the standard tetrahedral (*T*–4) arrangement of thf molecules around the Li^+ ion as found in other cases [14]. The structure of the $[Cr^{III}(C_6H_3Cl_2\text{-}2,6)_4]^-$ anion is depicted in Fig. 2 and a selection of interatomic distances

Table 1
Summary of crystallographic data and structure refinement for **1** and **2**

	1	**2**
Empirical formula	$C_{40}H_{44}Cl_8CrLiO_4$	$C_{24}H_{12}Cl_8Cr$
FW	931.29	635.94
T (K)	150(2)	150(2)
λ (pm)	71.073	71.073
Crystal system	Orthorhombic	Monoclinic
Space group	$P2_12_12_1$	$P2_1/c$
a (pm)	1472.12(17)	1053.6(4)
b (pm)	1478.06(11)	1093.9(3)
c (pm)	1955.51(18)	2079.5(5)
β (°)	90	92.31(2)
V (nm^3)	4.2550(7)	2.3947(12)
Z	4	4
d_c (g cm^{-3})	1.454	1.764
F(000)	1916	1264
Diffractometer	Enraf Nonius CAD4	
μ (mm^{-1})	0.811	1.384
θ Range (°)	2.08–24.99	2.10–24.98
Index range	$0 \leqslant h \leqslant 17$	$0 \leqslant h \leqslant 12$
	$0 \leqslant k \leqslant 17$	$0 \leqslant k \leqslant 12$
	$-23 \leqslant l \leqslant 23$	$-24 \leqslant l \leqslant 24$
Number of reflections collected	6407	5967
Number of unique reflections	5964 ($R_{int} = 0.0448$)	4170 ($R_{int} = 0.2009$)
refinement method	Full-matrix least-squares on F^2	
Final R indices $[I > 2\sigma(I)]$[a]	$R_1 = 0.0543$, $wR_2 = 0.1109$	$R_1 = 0.0848$, $wR_2 = 0.1203$
R indices (all data)	$R_1 = 0.1094$, $wR_2 = 0.1303$	$R_1 = 0.2645$, $wR_2 = 0.1599$
Goodness-of-fit on F^2[b]	1.008	0.982

[a] $R_1 = \sum(|F_o| - |F_c|)/\sum|F_o|$; $wR_2 = [\sum w(F_o^2 - F_c^2)^2/\sum w(F_c^2)^2]^{1/2}$; $w = [\sigma^2(F_o^2) + (g_1P)^2 + g_2P]^{-1}$; $P = (1/3)\cdot[\max\{F_o^2,0\} + 2F_c^2]$.
[b] Goodness-of-fit $= [\sum w(F_o^2 - F_c^2)^2/(n_{obs} - n_{param})]^{1/2}$.

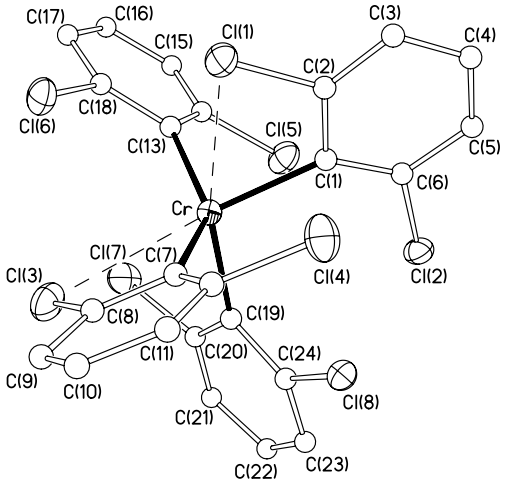

Fig. 2. Thermal ellipsoid diagram (50% probability) of the anion of **1**.

and angles is given in Table 2. The Cr^{III} center is surrounded by four 2,6-dichlorophenyl groups with Cr–C distances comprised between 208.1(7) and 215.7(7) pm. The presence of *ortho*-Cl substituents in the aryl group enables it to act as a poor chelate ligand by establishing secondary bonding interactions with the metal atom in two of the four 2,6-dichlorophenyl rings, thus rendering a six-coordinate Cr^{III} center. The two short $Cr\cdots Cl^{ortho}$ contacts [Cr···Cl(1) 287.5(2) pm and Cr···Cl(3) 299.2(3) pm] make the corresponding aryl rings swing sidewards as evidenced by the significantly different $Cr–C^{ipso}–C^{ortho}$ angles within each ring: Cr–C(1)–C(2) 110.0(5)° *vs.* Cr–C(1)–C(6) 137.7(5)° and Cr–C(7)–C(8) 111.0(5)° *vs.* Cr–C(7)–C(12) 136.7(7)°. No elongation of the corresponding $C^{ortho}–Cl^{ortho}$ bonds is observed. The C(19)-to-C(24) ring can be considered as a typically monodentate aryl ligand, since its two $Cr–C^{ipso}–C^{ortho}$ angles are equal within the experimental error [Cr–C(19)–C(20) 125.4(5)° and Cr–C(19)–C(24) 123.3(5)°] and the two *ortho*-Cl substituents are practically equidistant from the metal center (345.0 and 351.1 pm). Although the C(13)-to-C(18) ring is appreciably swung [Cr–C(13)–C(14) 129.8(5)° *vs.* Cr–C(13)–C(18) 118.7(6)°], the corresponding *ortho*-Cl substituents are too far from the metal center (>329 pm) to be considered as indicative of any bonding interaction.

The four σ-bonded C atoms and the two weakly interacting *ortho*-Cl atoms define a heavily distorted octahedron (*OC*-6) around the Cr^{III} center with a fairly large value of continuous shape measure, $S(OC\text{-}6) = 7.65$ [15–18]. The formation of two strained four-membered metallacycles with small $C^{ipso}–Cr–Cl^{ortho}$ angles [C(1)–Cr–Cl(1) 63.0(2)° and C(7)–Cr–Cl(3) 60.6(2)°] is the main source for distortion in the coordination polyhedron. Thus, the remaining angles between *cis* donor atoms are between 77.2(2)° and 113.73(7)°, while the angles between *trans* standing atoms are comprised between 143.3(2)° and 168.6(2)°. The overall structure of the $[Cr^{III}(C_6H_3Cl_2\text{-}2,6)_4]^-$ anion is quite similar to that observed for the perchlorophenyl homologous species $[Cr^{III}(C_6Cl_5)_4]^-$ [3]. The metal environment in the former is, however, slightly less distorted than in the latter, for which an even larger value of continuous shape measure was obtained, $S(OC\text{-}6) = 8.95$ [15–17].

Table 2
Selected bond distances and angles and their estimated standard deviations for $[Li(thf)_4][Cr(C_6H_3Cl_2\text{-}2,6)_4]$ (**1**)

Bond distances (pm)	
Cr–C(1)	208.1(7)
Cr–C(7)	215.0(7)
Cr–C(13)	215.7(7)
Cr–C(19)	209.8(7)
Cr···Cl(1)	287.5(2)
Cr···Cl(3)	299.2(3)
C(1)–C(2)	138.9(9)
C(1)–C(6)	138.2(10)
C(2)–Cl(1)	177.2(7)
C(6)–Cl(2)	174.7(7)
C(7)–C(8)	138.6(10)
C(7)–C(12)	138.9(10)
C(8)–Cl(3)	176.4(8)
C(12)–Cl(4)	176.1(8)
C(13)–C(14)	138.6(10)
C(13)–C(18)	139.0(10)
C(14)–Cl(5)	176.6(7)
C(18)–Cl(6)	177.4(8)
C(19)–C(20)	139.8(10)
C(19)–C(24)	140.4(10)
C(20)–Cl(7)	176.2(7)
C(24)–Cl(8)	175.5(7)
Bond angles (°)	
C(1)–Cr–C(7)	108.0(3)
C(1)–Cr–C(13)	93.9(3)
C(1)–Cr–C(19)	104.3(3)
C(1)–Cr–Cl(1)	63.0(2)
C(1)–Cr–Cl(3)	168.6(2)
C(7)–Cr–C(13)	143.3(3)
C(7)–Cr–C(19)	95.2(3)
C(7)–Cr–Cl(1)	82.9(2)
C(7)–Cr–Cl(3)	60.6(2)
C(13)–Cr–C(19)	107.7(3)
C(13)–Cr–Cl(1)	81.5(2)
C(13)–Cr–Cl(3)	96.4(2)
C(19)–Cr–Cl(1)	165.4(2)
C(19)–Cr–Cl(3)	77.2(2)
Cl(1)–Cr–Cl(3)	113.73(7)
Cr–C(1)–C(2)	110.0(5)
Cr–C(1)–C(6)	137.7(5)
C(2)–C(1)–C(6)	112.3(7)
C(1)–C(2)–Cl(1)	115.1(6)
C(1)–C(6)–Cl(2)	122.9(6)
Cr–C(7)–C(8)	111.0(5)
Cr–C(7)–C(12)	136.7(7)
C(8)–C(7)–C(12)	112.0(7)
C(7)–C(8)–Cl(3)	116.9(6)
C(7)–C(12)–Cl(4)	119.9(7)
Cr–C(13)–C(14)	129.8(5)
Cr–C(13)–C(18)	118.7(6)
C(14)–C(13)–C(18)	111.4(7)
C(13)–C(14)–Cl(5)	119.0(5)
C(13)–C(18)–Cl(6)	118.5(6)
Cr–C(19)–C(20)	125.4(5)
Cr–C(19)–C(24)	123.3(5)
C(20)–C(19)–C(24)	111.3(6)
C(19)–C(20)–Cl(7)	120.3(6)
C(19)–C(24)–Cl(8)	120.3(6)

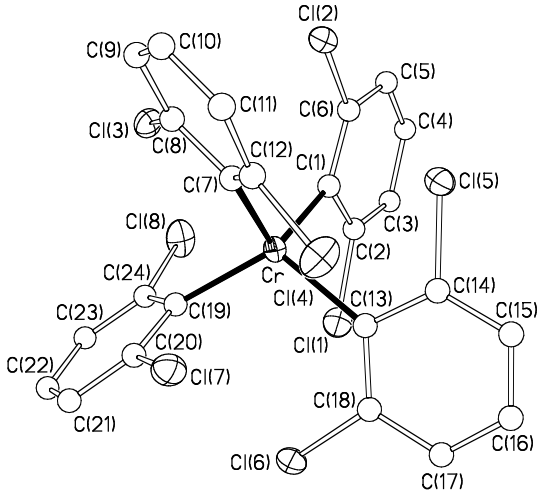

Fig. 3. Thermal ellipsoid diagram (50% probability) of **2**.

The structure of the neutral species $[Cr^{IV}(C_6H_3Cl_2\text{-}2,6)_4]$ (**2**) is depicted in Fig. 3, where it can be seen that the Cr^{IV} center forms just four Cr–C σ-bonds. The Cr^{IV}–C distances are between 203.2(11) and 205.0(11) pm, well in the range of the structurally characterized $[Cr^{IV}R_4]$ related species ($R = CH_2CMe_3$ [19], CH_2CMe_2Ph [20], Cy [21] and $CPh{=}CMe_2$ [22]). These Cr^{IV}–C distances in **2** are shorter than the corresponding Cr^{III}–C distances in **1** as expected for the different oxidation state of the metal center in each case. The coordination polyhedron in **2** can be described as a quite regular tetrahedron (*T*-4) with a very small value of continuous shape measure, $S(T\text{-}4) = 0.06$ [15–17]. A closer look at the structure, however, reveals a clear elongation of the *T*-4, as two of the C–Cr^{IV}–C angles are smaller than expected for the ideal geometry (109.5°), while the remaining four are larger (Table 3). In order to explain this distortion it is not necessary to invoke electronic effects associated with the d^2 electron configuration of the Cr^{IV} center. Similar distortions have also been found in other homoleptic, neutral $[M^{IV}(C_6Cl_5)_4]$ species with closed-shell (d^0 or d^{10}) electron configurations (M = Ti, Sn [23]) as well as in related $[M^{III}(C_6Cl_5)_4]^-$ anions (M = Ti [24], V [25]) with open-shell electron configurations (d^1 for Ti^{III} and d^2 for V^{III}). Such distortions have been attributed to steric problems in arranging four bulky and highly anisotropic aryl groups, R, around the metal center in a *T*-4 shape.

Table 3
Selected bond distances and angles and their estimated standard deviations for $[Cr(C_6H_3Cl_2\text{-}2,6)_4]$ (**2**)

Bond distances (pm)	
Cr–C(1)	204.1(11)
Cr–C(7)	203.2(11)
Cr–C(13)	203.6(11)
Cr–C(19)	205.0(11)
C(1)–C(2)	140.6(15)
C(1)–C(6)	139.4(15)
C(2)–Cl(1)	174.7(11)
C(6)–Cl(2)	177.0(12)
C(7)–C(8)	141.9(14)
C(7)–C(12)	137.2(14)
C(8)–Cl(3)	173.8(12)
C(12)–Cl(4)	174.0(11)
C(13)–C(14)	138.2(14)
C(13)–C(18)	140.5(15)
C(14)–Cl(5)	177.0(12)
C(18)–Cl(6)	173.4(11)
C(19)–C(20)	138.4(14)
C(19)–C(24)	140.0(15)
C(20)–Cl(7)	177.2(11)
C(24)–Cl(8)	171.7(12)
Bond angles (°)	
C(1)–Cr–C(7)	112.3(5)
C(1)–Cr–C(13)	101.2(4)
C(1)–Cr–C(19)	115.5(4)
C(7)–Cr–C(13)	111.7(5)
C(7)–Cr–C(19)	102.4(5)
C(13)–Cr–C(19)	114.2(5)
Cr–C(1)–C(2)	114.1(8)
Cr–C(1)–C(6)	132.8(9)
C(2)–C(1)–C(6)	112.9(10)
C(1)–C(2)–Cl(1)	118.7(9)
C(1)–C(6)–Cl(2)	119.2(9)
Cr–C(7)–C(8)	114.5(8)
Cr–C(7)–C(12)	130.6(9)
C(8)–C(7)–C(12)	114.9(10)
C(7)–C(8)–Cl(3)	118.1(9)
C(7)–C(12)–Cl(4)	123.4(9)
Cr–C(13)–C(14)	116.7(9)
Cr–C(13)–C(18)	128.5(8)
C(14)–C(13)–C(18)	114.6(11)
C(13)–C(14)–Cl(5)	117.7(9)
C(13)–C(18)–Cl(6)	122.9(8)
Cr–C(19)–C(20)	117.2(9)
Cr–C(19)–C(24)	127.7(8)
C(20)–C(19)–C(24)	115.1(10)
C(19)–C(20)–Cl(7)	118.0(9)
C(19)–C(24)–Cl(8)	122.6(9)

2.3. EPR spectra of the homoleptic polychloroarylchromium compounds

The X-band EPR spectra of polycrystalline samples of **1** and **4** registered at liquid nitrogen temperature (77.3 K) are shown in Fig. 4 together with that of the related species $[Li(thf)_4][Cr^{III}(C_6Cl_5)_4]$ for comparison purposes. On the right side of this figure, calculated spectra are shown considering a spin $S' = 1/2$ and the principal g'_i values ($i = 1$, 2, 3) given in Table 4. The observed features can be interpreted as due to an $S = 3/2$ paramagnetic species with apparent spin $S' = 1/2$ and an orthorhombic effective $\tilde{\mathbf{g}}'$ tensor as will be commented on briefly.

The fundamental term for the free Cr^{III} ion (*i.e.*, a d^3 ion under spherical symmetry) is the quartet ^4F ($S = 3/2$). When located in an octahedral environment, this term splits into two orbital triplets ($^4T_2$ and $^4T_1$) plus an orbital singlet, $^4A_2$, which becomes the fundamental term under this symmetry field. To describe the magnetic properties of our Cr^{III} systems through their corresponding spin Hamiltonian, the low-field limit approximation has proven to be particularly suitable [3]. In this case, the zero field

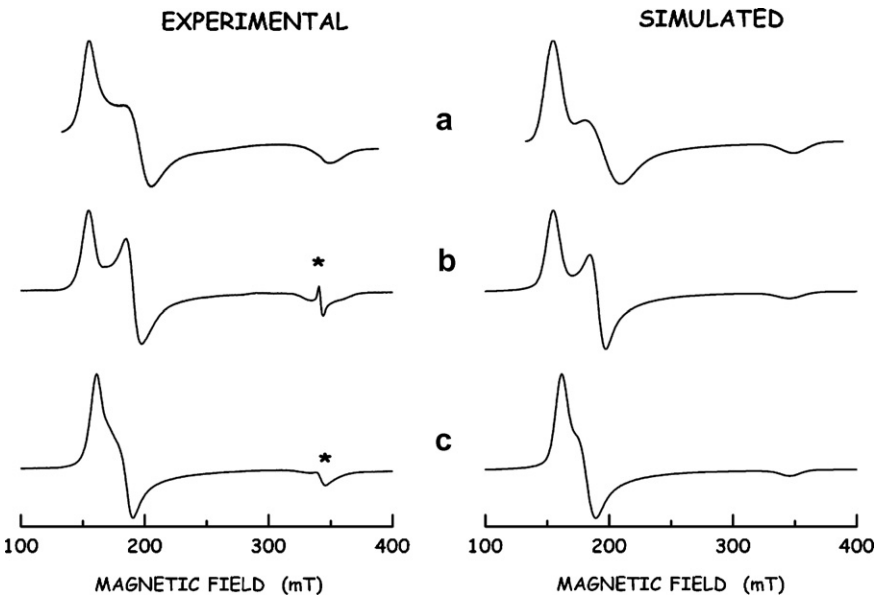

Fig. 4. Liquid nitrogen experimental (left) and simulated (right) X-band EPR spectra of powder samples of the following compounds: $[Li(thf)_4][Cr^{III}(C_6Cl_5)_4]$ (a), $[Li(thf)_4][Cr^{III}(C_6H_3Cl_2\text{-}2,6)_4]$ (b), and $[NBu_4][Cr^{III}(C_6Cl_5)_4]$ (c). Every spectrum was measured up to 1.5 T but no additional signals were detected above the magnetic field indicated in the trace. The starred signal at $g \approx 2.00$ is assigned to some minoritary radical species.

Table 4
Relevant electronic parameters derived from the analyses of the EPR spectra of polycrystalline samples of the homoleptic polychloroaryl Cr^{III} (d^3) derivatives registered at 77.3 K

Compound	g'_1	g'_2	g'_3	g	η
$[Li(thf)_4][Cr^{III}(C_6Cl_5)_4]$[a]	4.377	3.456	1.943	1.968	0.079
$[Li(thf)_4][Cr^{III}(C_6H_3Cl_2\text{-}2,6)_4]$ (**1**)	4.385	3.550	1.960	1.991	0.070
$[NBu_4][Cr^{III}(C_6Cl_5)_4]$ (**4**)	4.200	3.725	1.960	1.982	0.040

[a] See Ref. [3]. The effective principal g-values obtained in frozen CH_2Cl_2 solutions are as follows: $g'_x = 4.02$, $g'_y = 3.55$ and $g'_z = 1.946$, which give a value for the orthorhombicity parameter $\eta = 0.08$.

splitting (ZFS) term within the spin Hamiltonian, $H_{ZFS} = \mathbf{S} \cdot \widetilde{\mathbf{D}} \cdot \mathbf{S}$, is the dominant one, while the Zeeman term, $H_{Ze} = \mu_B \mathbf{B} \cdot \tilde{\mathbf{g}} \cdot \mathbf{S}$, can be treated merely as a perturbation thereof. In this kind of approximation, H_{ZFS} is taken as a 0th-order term and can be written with respect to its principal axes (X, Y, Z) as

$$H_{ZFS} = \mathbf{S} \cdot \widetilde{\mathbf{D}} \cdot \mathbf{S} = D\left[S_Z^2 - \frac{1}{3}S(S+1) + \eta(S_X^2 - S_Y^2)\right]. \quad (1)$$

This means that, even in the absence of any applied magnetic field, the four spin states associated with the fundamental term $^4A_2$ split into two Kramers doublets $\{\Psi_{\pm 1/2}\}$ and $\{\Psi_{\pm 3/2}\}$, separated by an energy difference $\Delta E = 2D\sqrt{1+3\eta^2}$. In the low-field approximation, the ΔE value is significantly larger than the energy resulting from the electronic Zeeman interaction and hence, the two Kramers doublets can be considered as completely independent systems with regard to the EPR spectroscopy. As a result, each of these Kramers doublets can be assigned an apparent spin $S' = 1/2$ and is described by an effective $\tilde{\mathbf{g}}'$ tensor, which is itself a function of the true $\tilde{\mathbf{g}}$ tensor associated with the $(S = 3/2)$-system as well as of the orthorhombicity parameter η. In the low-field approximation and according to the selection rule $|\Delta m_s| = 1$, the spectrum should contain mainly transitions within the $\{\Psi_{\pm 1/2}\}$ doublet. Assuming that the principal axes of the $\tilde{\mathbf{g}}$ and $\widetilde{\mathbf{D}}$ tensors coincide, the relationship between the apparent g'_i values within the $\{\Psi_{\pm 1/2}\}$ doublet and the true g_i values, are given by

$$g'_x = g_x\left(1 + \frac{1-3\eta}{\sqrt{1+3\eta^2}}\right),$$

$$g'_y = g_y\left(1 + \frac{1+3\eta}{\sqrt{1+3\eta^2}}\right),$$

$$g'_z = g_z\left(\frac{2}{\sqrt{1+3\eta^2}} - 1\right).$$

It is reasonable to assume that the introduction of geometric distortions in the octahedral environment of the Cr^{III} paramagnetic center will induce additional splitting in the excited states only, as the fundamental one is an orbital singlet. If the low symmetry effects and hence the anisotropy induced in the true $\tilde{\mathbf{g}}$ tensor are not very large, we can still make use of an isotropic g factor (*i.e.* $g_x = g_y = g_z = g$). Thus, a set of g'_i values could in principle be derived from any given couple of g and η values taking $g'_1 = g'_y$, $g'_2 = g'_x$ and $g'_3 = g'_z$.

Following this reasoning, the estimated values of g and η yielding the set of g'_i values best fitting the experimental spectra are given in Table 4. The values thus derived for the isotropic g factor are close to that of the free electron $[g_e = 2.0037(2)]$, as is generally observed in other Cr^{III} species. The value of the orthorhombicity parameter η for **1** is

similar to that obtained for the homologous pentachlorophenyl derivative $[Li(thf)_4][Cr^{III}(C_6Cl_5)_4]$: 0.070 *vs.* 0.079 [3a]. This observation is in keeping with the similar geometric environment found for the Cr^{III} center in the two $[Li(thf)_4][Cr^{III}R_4]$ salts ($R = C_6H_3Cl_2$-2,6 and C_6Cl_5). A smaller value of η was observed for the salt $[NBu_4][Cr^{III}(C_6Cl_5)_4]$ (**4**; Table 4). Pronounced effects in the EPR parameters had already been reported to occur in systems with $S > 1/2$ (as is the case of the Cr^{III} ion) caused by small changes in the surroundings of the paramagnetic center, which include lattice effects derived from the nature of the counterion [26]. Also the temperature is known to induce modifications in the ZFS contribution through the spin coupling to the lattice vibrations [27]. In fact, the EPR spectra of **1** and **4** are observed to broaden on rising the temperature—the two low-field features becoming unresolved. Careful simulation of these spectra is still possible, allowing us to infer a decrease of η as the temperature increases. However, the specific value of D cannot be determined from these EPR spectra.

The room temperature EPR spectrum of **2** is shown in Fig. 5. No significant modifications are observed when the temperature goes down to 10 K. The spectrum is similar to but still broader than that observed for the homologous species $[Cr^{IV}(C_6Cl_5)_4]$ [3a]. Since, in the case of non-Kramers systems, this type of spectra is poorly informative, the magnetic characterization of **2** will rely mainly on magnetism measurements (see below).

2.4. Magnetism measurements

The spin states of the 2,6-dichlorophenyl compounds **1** and **2** have been established by isothermal dc magnetization measurements, M(H), at low temperatures (Fig. 6). The saturation tendency at 1.8 K indicate spin states $S = 3/2$ and $S = 1$ for the Cr^{III} (**1**; d^3) and Cr^{IV} (**2**; d^2) species, respectively. The magnetic behavior of **4** is practically superimposable to that of **1** and hence, it is not given in the figures for the sake of clarity. The fact that the plots at different temperatures given in Fig. 6 do not fit a universal curve can be interpreted as a further manifestation of the ZFS effect already invoked to explain the EPR spectra of the Cr^{III} compounds. Accordingly, a simple Curie law cannot be used to describe the thermal evolution of the in-phase ac magnetic susceptibility of these compounds, $\chi(T)$, as already noted for the related compounds $[Li(thf)_4][Cr^{III}(C_6Cl_5)_4]$ and $[Cr^{IV}(C_6Cl_5)_4]$ [3a]. As in those cases, a polynomial expansion of $\chi(T)$ in powers of T^{-1} has been used for analyzing the data shown in Fig. 7:

$$\chi(T) = \chi_0 + \frac{C}{T}\left(1 + \frac{k_1}{T} + \frac{k_2}{T^2} + \cdots\right), \qquad (2)$$

where χ_0 accounts for the temperature independent contribution to the magnetic susceptibility, χ_{TIP}—including the diamagnetic contribution—, C is the Curie constant for a simple paramagnet, and k_j ($j = 1, 2, \ldots$) are constants containing information on the ZFS contribution. Dashed lines

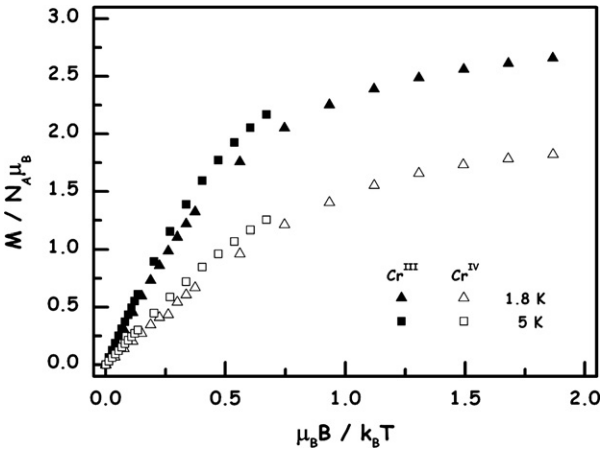

Fig. 6. Dependence of the dc magnetization, $M/N_A\mu_B$, *vs.* the reduced applied magnetic field ($\mu_B B/k_B T$) of **1** (solid symbols) and **2** (open symbols) measured at 1.8 K (triangles) and 5 K (squares).

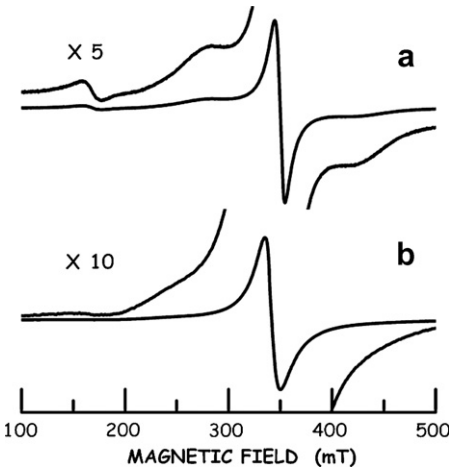

Fig. 5. Room temperature X-band EPR spectra of powder samples of $[Cr^{IV}(C_6Cl_5)_4]$ (a) and $[Cr^{IV}(C_6H_3Cl_2\text{-}2,6)_4]$ (b).

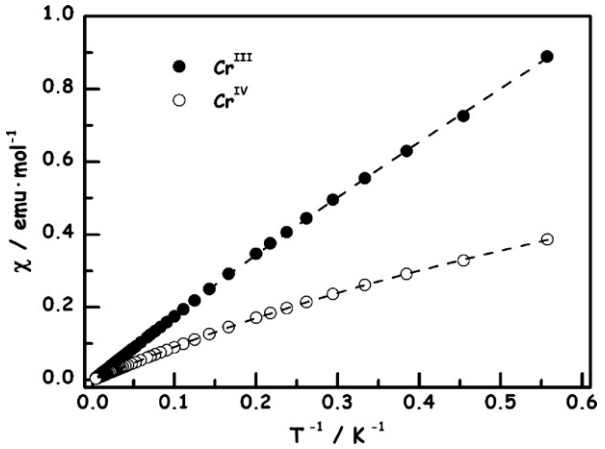

Fig. 7. AC magnetic susceptibility of **1** (filled circles) and **2** (empty circles) as a function of the inverse of temperature. The dashed lines represent the fit of Eq. (2) truncated in the T^{-3} term (see text).

in Fig. 7 correspond to a fit of the experimental data of $\chi(T)$ *vs.* T^{-1} (filled or empty circles) to this polynomial expansion truncated in the T^{-3} term. The values thus obtained for C and for the high-temperature magnetic moment per molecule, μ_∞, are collected in Table 5 together with the estimated g values.

Plots of $\mu(T)$ *vs.* T for compounds **1** and **2** are given in Fig. 8. In the absence of ZFS contribution, μ should be temperature independent. However, significant departures from this "horizontal" behavior are observed for both compounds at low temperatures. In the case of an $S = 3/2$ entity, and assuming that the principal axes of the $\tilde{\mathbf{g}}$ and $\widetilde{\mathbf{D}}$ tensors coincide, the following expression can easily be derived:

$$\mu(T) = \mu_B \left[C_1 + C_2 \left(\frac{2k_B T}{\Delta E} \right) \tanh \left(\frac{\Delta E}{2k_B T} \right) + C_3 \tanh \left(\frac{\Delta E}{2k_B T} \right) \right]^{1/2}, \quad (3)$$

where $\Delta E = 2D(1 + 3\eta^2)^{1/2}$ as above. The solid line in Fig. 8 (upper trace) represents the best fit of this expression to the **1** data, obtained for $\Delta E = 191(31)$ GHz. A similar analysis of the data corresponding to **4** and $[Li(thf)_4][Cr^{III}(C_6Cl_5)_4]$ (not shown in the Figure), yielded the values $\Delta E = 142(10)$ GHz and $\Delta E = 75(4)$ GHz, respectively. It is interesting to note that in all these cases, the splitting between the $\{\Psi_{\pm 1/2}\}$ and $\{\Psi_{\pm 3/2}\}$ doublets is higher than the microwave frequency, in agreement with our interpretation of the EPR data (see above).

Table 5
Parameters derived from magnetization measurements

Compound	C [emu mol^{-1} K]	μ_∞ [μ_B]	S	$\sqrt{\langle g^2 \rangle}$	g_{EPR}
$[Li(thf)_4][Cr^{III}(C_6H_3Cl_2$-2,6)$_4]$ (**1**)	1.85(1)	3.85	3/2	1.986	1.991
$[Cr^{IV}(C_6H_3Cl_2$-2,6)$_4]$ (**2**)	0.972(4)	2.89	1	1.972	–
$[NBu_4][Cr^{III}(C_6Cl_5)_4]$ (**4**)	1.82(2)	3.91	3/2	1.970	1.982

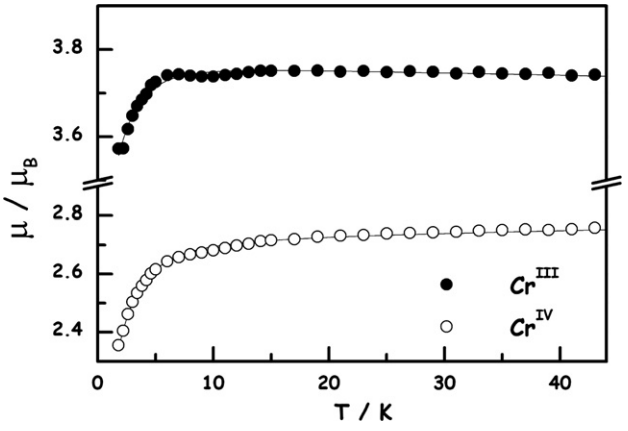

Fig. 8. Effective magnetic moment per molecule in the low-field region (linear region) as a function of temperature for **1** (solid symbols) and **2** (open symbols). Solid lines represent the evolution predicted according to Eqs. (3) and (4) in each case (see text).

In the case of a non-Kramers $S = 1$ entity (Cr^{IV}), and assuming again coaxiality of the $\tilde{\mathbf{g}}$ and $\widetilde{\mathbf{D}}$ tensors, it is also possible to derive a suitable expression relating $\mu(T)$ with the ZFS parameters D and η. Since $\mu(T)$ was found to be practically insensitive to variations of η, it is convenient to consider an axial case ($\eta = 0$). Under all these assumptions, and neglecting any anisotropic contribution to the $\tilde{\mathbf{g}}$ tensor, the following expression is obtained [28]:

$$\mu(T) = g \left[\frac{4d^{-1}(1 - e^{-d}) + 2e^{-d}}{2e^{-d} + 1} \right]^{1/2}, \quad (4)$$

where $d = D/k_B T$. A fit of this expression to the experimental data of **2** gave $g = 1.912(2)$ and $D = -139(2)$ GHz as the values yielding the best agreement (solid line in the lower trace of Fig. 8). A similar analysis of the previously reported $[Cr^{IV}(C_6Cl_5)_4]$ data [3a] gave the following optimized values: $g = 1.850(1)$ and $D = -46.7(8)$ GHz.

2.5. Synthesis and characterization of $[Li(thf)_4][Mo^VO(C_6Cl_5)_4]$ (**5**)

We have tried to prepare homoleptic haloaryl-derivatives of molybdenum. However, all our attempts using different Mo starting products and arylating conditions have failed so far: either unidentified reaction products were obtained or unreacted starting materials were recovered from the reaction medium. Only by reaction of $[MoCl_4(dme)]$ with LiC_6Cl_5 in Et_2O was a defined product obtained, which was identified as $[Li(thf)_4][Mo^VO(C_6Cl_5)_4]$ (**5**). Compound **5** results from a combined process entailing both arylation and oxidation of the metal center (Eq. (5)).

$$[MoCl_4(dme)] + LiC_6Cl_5 \xrightarrow{+thf} \underset{\textbf{5},\ \text{garnet},\ 40\%\ \text{yield}}{[Li(thf)_4][Mo^VO(C_6Cl_5)_4]} \quad (5)$$

Complex **5** was identified by analytical and spectroscopic methods. The MS (FAB−) shows a peak corresponding to the parent species $[Mo^VO(C_6Cl_5)_4]^-$ (m/z 1102) together with various anionic fragments derived thereof, all of them showing the appropriate isotopic pattern for the suggested stoichiometry. An absorption in the IR spectrum of **5** attributable to the ν(Mo=O) mode could not be unambiguously assigned due to the rich vibrational pattern of both the C_6Cl_5 groups and the thf molecule. Information about the geometry of the $[Mo^VO(C_6Cl_5)_4]^-$ anion was obtained from the combination of X-ray diffraction data and EPR spectroscopic results.

Poor-quality single crystals of $[Li(C_8H_{16}O_4)_2][Mo^VO(C_6Cl_5)_4]$ (**5′**; $C_8H_{16}O_4$ = 12-crown-4 ether) were obtained, but the X-ray diffraction data collected were not of sufficient quality to carry out a complete structural determination of the complex. Nevertheless, its general shape and the connectivity could be established [29]. The geometry of the $[Mo^VO(C_6Cl_5)_4]^-$ anion, depicted in Fig. 9, can be described as square-pyramidal (*SPY*-5) with the C_6Cl_5 groups hellicoidally arranged in the basal plane and the

oxygen atom located in the apex of the pyramid. This coordination environment is similar to that found for the related $[Mo^{V}OX_4]^-$ anions (X = Cl, Br, I) [30]. The protecting effect of the bulky C_6Cl_5 groups can reasonably account for the stability of this base-free, five-coordinate species, which shows no tendency to coordinate a further ligand rendering a more saturated, six-coordinate derivative.

The EPR spectrum of a polycrystalline sample of **5** (Fig. 10) shows no temperature dependence within the 120–300 K range. It can be assigned to a $S = 1/2$ entity with an axial $\tilde{\mathbf{g}}$ tensor with the following principal values: $g_{\|} = 1.996(1)$ and $g_{\perp} = 1.969(1)$. The calculated spectrum using these values and a lorentzian lineshape with peak-to-peak separations of $\Delta Hpp(\|) = 1.7$ mT and $\Delta Hpp(\perp) = 0.7$ mT is also shown in Fig. 10.

Based on a raw crystal-field model, the ground-state orbital for a *SPY*-5 species such as the $[Mo^{V}O(C_6Cl_5)_4]^-$ anion (ideal C_{4v} symmetry), should be expected to be the d_{xy} one with the following relative values for the corresponding $\tilde{\mathbf{g}}$ tensor: $g_{\|} < g_{\perp} < g_e$. This behavior has indeed been observed in highly ionic species such as the $[Mo^{V}OF_4]^-$ anion and other oxofluoromolybdenum derivatives [31]. Our experimental results for complex **5**, however, show the opposite trend, *i.e.*, $g_{\perp} < g_{\|}$. This "inverted" situation had already been found to occur in several oxomolybdenum derivatives including the closely related $[Mo^{V}OCl_4]^-$ anion [30] as well as the series of six-coordinate anions $[Mo^{V}OX_5]^{2-}$ (X = Cl, Br, I). The different approaches taken to explain this "inverted" behavior point to metal-ligand covalency as the main factor causing it [32]. The C_6Cl_5 group is considered to have an electron-withdrawing effect, that is weaker than that assigned to the Cl atom [33]. Given this relationship, the EPR spectroscopic properties of **5** can also be rationalized in terms of the Mo–C_6Cl_5 bond covalency.

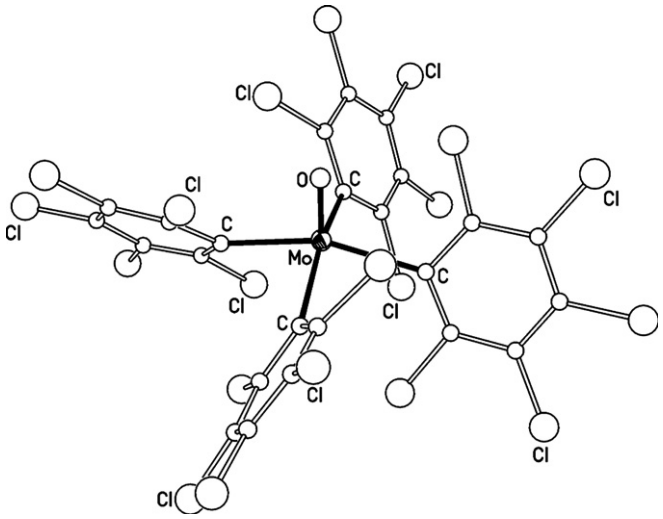

Fig. 9. Schematic drawing of the anion of **5**.

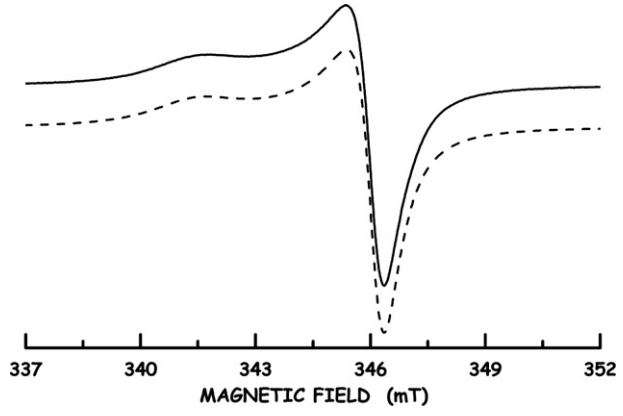

Fig. 10. Experimental (solid line) and simulated (dashed line) X-band EPR spectrum of a powder sample of **5** at 120 K.

3. Concluding remarks

We have demonstrated that the 2,6-dichlorophenyl group is also able to establish secondary bonding interactions with the metal center through one of its *ortho*-Cl substituents, thus acting as a poor chelating ligand, $C_6H_3Cl_2$-2,6-$\kappa C,\kappa Cl^2$. The presence of just two highly electronegative Cl substituents in the phenyl ring makes it markedly less electron-withdrawing in character than the analogous perchlorinated group C_6Cl_5. This difference is evidenced by the potential, $E_{1/2}$, of the one-electron exchange process operating in the $[Cr^{IV}R_4]/[Cr^{III}R_4]^-$ couple, which drops from 0.76 V when $R = C_6Cl_5$ to 0.16 V when $R = C_6H_3Cl_2$-2,6. Given also the different solubility of the metal complexes containing these two polychlorophenyl groups under consideration, they can be used to induce the desired global properties in the final compound.

According to the similar geometries observed for the $[Cr^{III}R_4]^-$ anions (pseudo *OC*-6), the d^3 Kramers salts $[Li(thf)_4][Cr^{III}R_4]$ have been found to behave as $S = 3/2$ species with similar magnetic properties—both macroscopic (bulk magnetization measurements) and microscopic (EPR). The *T*-4 derivative $[Cr^{IV}(C_6H_3Cl_2\text{-}2,6)_4]$ (**2**) has a magnetism corresponding to an $S = 1$ species.

Finally, a *SPY*-5 geometry has been established for the d^1 ($S = 1/2$) anion $[Mo^{V}O(C_6Cl_5)_4]^-$ by the combined analysis of EPR spectroscopic and X-ray diffractometric data.

4. Experimental

All reactions and manipulations were carried out under purified argon using Schlenk techniques. Solvents were dried by standard methods and distilled prior to use. The metal complexes $[CrCl_3(thf)_3]$ [34], $[Cr^{IV}(C_6Cl_5)_4]$ [3a], and $[MoCl_4(dme)]$ [35] as well as the organolithium reagents $LiC_6H_3Cl_2$-2,6 [13b] and LiC_6Cl_5 [36] were prepared as described elsewhere. The aminium salt $[N(C_6H_4Br\text{-}4)_3][SbCl_6]$ was purchased (Aldrich) and used as received. Elemental analyses were carried out with a Perkin–Elmer 2400-Series II microanalyzer. IR spectra of KBr discs were recorded on a Perkin–Elmer 883 spectropho-

tometer in the range 4000–200 cm^{-1}. Mass spectra were recorded on a VG-Autospec spectrometer using the standard Cs-ion FAB (acceleration voltage: 35 kV).

4.1. Synthesis of $[Li(thf)_4][Cr^{III}(C_6H_3Cl_2\text{-}2,6)_4]$ (1)

$[CrCl_3(thf)_3]$ (1.04 g, 2.77 mmol) suspended in Et_2O (20 cm^3) at −78 °C was stepwise added *via* cannula to a suspension of $LiC_6H_3Cl_2$-2,6 (*ca.* 16.6 mmol) in Et_2O (50 cm^3) under stirring. The temperature of the reaction mixture was allowed to rise to 0 °C and then maintained for 3 h in an ice bath. At this point a violet solid had formed, which was filtered, washed with Et_2O (3×5 cm^3) and extracted in CH_2Cl_2 (70 cm^3) at 0 °C. The extract was concentrated to dryness and the resulting residue was treated with thf (20 cm^3). The violet solid formed (**1**) was filtered, washed with Et_2O (5 cm^3) and vacuum dried. Slow diffusion of a Et_2O (40 cm^3) layer onto the mother liquor at −30 °C gave a second fraction of **1**, which was thus isolated in 48% overall yield (1.25 g, 1.34 mmol). Anal. Found: C 50.2, H 4.75; $C_{40}H_{44}Cl_8CrLiO_4$ requires: C 51.6, H 4.8%. IR (KBr, cm^{-1}): $\tilde{\nu}_{max}$ 1577 (w), 1554 (m), 1539 (s), 1460 (m), 1399 (vs), 1247 (m), 1232 (sh), 1164 (m), 1118 (s), 1043 (vs; C–O–C_{asym}) [12], 918 (sh), 887 (s; C–O–C_{sym}) [12], 768 (vs), 751 (vs), 692 (m) and 683 (m). MS (FAB−): *m/z* 632 $[Cr(C_6H_3Cl_2\text{-}2,6)_4]^-$, 522 $[Cr(C_6H_3Cl_2\text{-}2,6)_3Cl]^-$, 487 $[Cr(C_6H_3Cl_2\text{-}2,6)_3]^-$, 412 $[Cr(C_6H_3Cl_2\text{-}2,6)_2Cl_2]^-$, and 377 $[Cr(C_6H_3Cl_2\text{-}2,6)_2Cl]^-$.

4.2. Synthesis of $[Cr^{IV}(C_6H_3Cl_2\text{-}2,6)_4]$ (2)

The addition of $[N(C_6H_4Br\text{-}4)_3][SbCl_6]$ (0.47 g, 0.57 mmol) to a solution of **1** (0.53 g, 0.57 mmol) in CH_2Cl_2 (15 cm^3) at 0 °C caused the immediate precipitation of a brown solid. After 30 min of further stirring in an ice bath, the solid was filtered, washed with CH_2Cl_2 (3×5 cm^3), and vacuum dried (**2**: 0.27 g, 0.43 mmol, 74% yield). Anal. Found: C 45.0, H 1.9; $C_{24}H_{12}Cl_8Cr$ requires: C 45.3, H 1.9%. IR (KBr, cm^{-1}): $\tilde{\nu}_{max}$ 1552 (w), 1542 (m), 1462 (w), 1404 (vs), 1245 (w), 1172 (m), 1137 (m), 1100 (w), 784 (m), 772 (vs), 765 (s), and 686 (w). MS (FAB−): *m/z* 632 $[Cr(C_6H_3Cl_2\text{-}2,6)_4]^-$, 522 $[Cr(C_6H_3Cl_2\text{-}2,6)_3Cl]^-$, 487 $[Cr(C_6H_3Cl_2\text{-}2,6)_3]^-$, 412 $[Cr(C_6H_3Cl_2\text{-}2,6)_2Cl_2]^-$, and 377 $[Cr(C_6H_3Cl_2\text{-}2,6)_2Cl]^-$.

4.3. Synthesis of $[NBu_4]_2[Cr^{II}(C_6Cl_5)_4]$ (3)

$[CrCl_3(thf)_3]$ (0.86 g, 2.29 mmol) suspended in Et_2O (15 cm^3) at −78 °C was stepwise added *via* cannula to a solution of LiC_6Cl_5 (*ca.* 11.5 mmol) in Et_2O (50 cm^3) under stirring. The temperature of the reaction mixture was allowed to rise and by *ca.* −35 °C, solid NBu_4Br (0.74 g, 2.29 mmol) was added. The whole mixture was allowed to reach 0 °C and then it was stirred for further 3 h in an ice bath. The salmon pink solid in suspension was filtered, washed with Et_2O (3×5 cm^3) and extracted in CH_2Cl_2 (60 cm^3) at 0 °C. Concentration of the extract to *ca.* 15 cm^3 caused the precipitation of a salmon pink solid (**3**) which was filtered and vacuum dried. Slow diffusion of a Et_2O (40 cm^3) layer onto the mother liquor at −30 °C gave a second fraction of **3**, which was thus isolated in 28.5% overall yield (1.00 g, 0.65 mmol). Anal. Found: C 43.0, H 4.2, N 1.7; $C_{56}H_{72}Cl_{20}CrN_2$ requires: C 43.8, H 4.7, N 1.8%. IR (KBr, cm^{-1}): $\tilde{\nu}_{max}$ 1306 (s), 1276 (vs), 1227 (m), 1041 (m), 880 (w; $[NBu_4]^+$), 808 (s; C_6Cl_5: X-sensitive vibration) [37], 739 (w; $[NBu_4]^+$), and 658 (s). MS (FAB−): *m/z* 1040 $[Cr(C_6Cl_5)_4]^-$, 828 $[Cr(C_6Cl_5)_3Cl]^-$, 616 $[Cr(C_6Cl_5)_2Cl_2]^-$, 581 $[Cr(C_6Cl_5)_2Cl]^-$, and 546 $[Cr(C_6Cl_5)_2]^-$.

4.4. Synthesis of $[NBu_4][Cr^{III}(C_6Cl_5)_4]$ (4)

To a solution of **3** (0.49 g, 0.32 mmol) in CH_2Cl_2 (40 cm^3) at 0 °C, was added solid $[Cr^{IV}(C_6Cl_5)_4]$ (0.34 g, 0.32 mmol). After 90 min stirring, the reaction mixture was concentrated to *ca.* 10 cm^3. Addition of *n*-hexane caused the precipitation of a violet solid, which was filtered and vacuum dried (**4**: 0.55 g, 0.43 mmol, 67.2% yield). Anal. Found: C 36.2, H 2.7, N 1.0; $C_{40}H_{36}Cl_{20}CrN$ requires: C 37.2, H 2.8, N 1.1%. IR (KBr, cm^{-1}): $\tilde{\nu}_{max}$ 1320 (s), 1309 (s), 1281 (vs), 1219 (w), 1058 (m), 881 (w; $[NBu_4]^+$), 822 (s; C_6Cl_5: X-sensitive vibration) [37], 739 (w; $[NBu_4]^+$), and 669 (s). MS (FAB−): *m/z* 1040 $[Cr(C_6Cl_5)_4]^-$, 828 $[Cr(C_6Cl_5)_3Cl]^-$, 793 $[Cr(C_6Cl_5)_3]^-$, 616 $[Cr(C_6Cl_5)_2Cl_2]^-$, 581 $[Cr(C_6Cl_5)_2Cl]^-$, and 546 $[Cr(C_6Cl_5)_2]^-$.

4.5. Synthesis of $[Li(thf)_4][Mo^{V}O(C_6Cl_5)_4]$ (5)

$[MoCl_4(dme)]$ (1.70 g, 4.45 mmol) suspended in Et_2O (10 cm^3) at −78 °C was stepwise added *via* cannula to a solution of LiC_6Cl_5 (*ca.* 22.3 mmol) in Et_2O (80 cm^3) under stirring. The suspension was allowed to warm up to 0 °C and after about 4 h of stirring, the by then red solid was filtered, washed with Et_2O (3×5 cm^3), and extracted in CH_2Cl_2 (50 cm^3) still at 0 °C. The extract was concentrated to dryness and the resulting residue was redissolved in thf (5 cm^3). The slow diffusion at −30 °C of a Et_2O layer (40 cm^3) into the preceding solution yielded **5** as a garnet solid (2.50 g, 1.78 mmol, 40% yield). Anal. Found: C 34.1, H 2.5; $C_{40}H_{32}Cl_{20}LiMoO_5$ requires: C 34.2, H 2.3%. IR (KBr, cm^{-1}): $\tilde{\nu}_{max}$ 2979 (m), 2883 (m), 1461 (w), 1314 (s), 1285 (vs), 1273 (vs), 1196 (w), 1133 (w), 1121 (m), 1066 (m), 1044 (s; C–O–C_{asym}) [12], 915 (sh), 889 (s; C–O–C_{sym}) [12], 829 (m; C_6Cl_5: X-sensitive vibration) [37], and 674 (s). MS (FAB−): *m/z* 1102 $[Mo(C_6Cl_5)_4O]^-$, 890 $[Mo(C_6Cl_5)_3ClO]^-$, 608 $[Mo(C_6Cl_5)_2O]^-$, and 396 $[Mo(C_6Cl_5)ClO]^-$.

4.6. Synthesis of $[Li(C_8H_{16}O_4)_2][Mo^{V}O(C_6Cl_5)_4]$ (5′)

By using the procedure described for the synthesis of **5**, compound **5′** was prepared starting from $[MoCl_4(dme)]$ (1.00 g, 3.05 mmol) and LiC_6Cl_5 (*ca.* 15.25 mmol). The

CH_2Cl_2 extract was concentrated to *ca.* 10 cm^3 and a few drops of 12-crown-4 ether ($C_8H_{16}O_4$) were added. The slow diffusion of a Et_2O layer (25 cm^3) into that solution yielded **5′** as a garnet solid (2.51 g, 1.71 mmol, 56% yield). Anal. Found: C 32.5, H 2.45; $C_{40}H_{32}Cl_{20}LiMoO_9$ requires: C 32.7, H 2.2%. IR (KBr, cm^{-1}): $\tilde{\nu}_{max}$ 2915 (m), 2872 (m), 1447 (w), 1365 (w), 1315 (s), 1285 (vs), 1273 (vs), 1245 (w), 1196 (w), 1135 (vs), 1098 (vs), 1066 (m), 1025 (s), 926 (m), 856 (m), 827 (m; C_6Cl_5: X-sensitive vibration) [37] and 674 (s). MS (FAB−): *m/z* 1102 $[Mo(C_6Cl_5)_4O]^-$, 1067 $[Mo(C_6Cl_5)_3(C_6Cl_4)O]^-$, 608 $[Mo(C_6Cl_5)_2O]^-$, and 396 $[Mo(C_6Cl_5)ClO]^-$.

4.7. X-ray crystallography

Crystal data and other details of the structure analyses of compounds **1** and **2** are presented in Table 1. Suitable crystals were mounted at the end of quartz fibers and held in place with a fluorinated oil. All diffraction measurements were made at 150 K on an Enraf-Nonius CAD-4 diffractometer, using graphite monochromated Mo Kα radiation. Unit cell dimensions were determined from 24 centered reflections in the range $20.9° < 2\theta < 28.2°$ for **1** and in the range $17.2° < 2\theta < 31.5°$ for **2**. For both structures, diffracted intensities were measured in a quarter of reciprocal space for $4.0° < 2\theta < 50.0°$ by ω scans in the case of **1**, and by ω/θ scans for **2**. Three check reflections remeasured after every 300 ordinary reflections showed no decay of the diffracted intensities over the period of data collection. Absorption corrections were applied based on azimuthal scan data (526 for **1** and 476 for **2**). Lorentz and polarization corrections were applied.

The structures were solved by direct methods and refined using the SHELXL-97 program [38]. All non-hydrogen atoms were assigned anisotropic displacement parameters. The hydrogen atoms were constrained to idealized geometries and assigned isotropic displacement parameters equal to 1.2 times the U_{iso} values of their respective parent atoms. In the case of **2**, due to the low intensity of the collected data, there were some problems with the anisotropic thermal parameters of the C(6), C(14), and C(22) atoms and thus, a common set of anisotropic thermal parameters were used for each of these atoms and their adjacent carbon neighbors. Full-matrix least-squares refinement of these models against F^2 converged to final residual indices given in Table 1.

4.8. EPR measurements

EPR data were taken in a Bruker ESP380 spectrometer working at X-band. Measurements at liquid nitrogen temperature (77.3 K) were registered using a quartz immersion Dewar. The magnetic field was measured with a Bruker ER035M gaussmeter. A Hewlett–Packard HP5350B frequency counter was used to determine the microwave frequency. The samples were introduced in fused quartz tubes.

4.9. Magnetic measurements

Magnetic measurements of polycrystalline samples were carried out using a Quantum Design SQUID-Based Magnetometer MPMS-XL5. The magnetometer was calibrated using standard palladium and dysprosium oxide reference samples supplied by Quantum Design. The accuracy of the measurements is better than 1%. Magnetic susceptibility measurements were performed from 1.8 to 265 K at 10 Hz and 4.1 Oe amplitude.

4.10. Electrochemistry

Electrochemical studies were carried out using an EG&G model 273 potentiostat in conjunction with a three-electrode cell, in which the working electrode was a platinum disc, the auxiliary electrode a platinum wire and the reference was an aqueous saturated calomel electrode (SCE) separated from the test solution by a fine-porosity frit and an agar bridge saturated with KCl. Where possible, solutions were 5×10^{-4} mol dm^{-3} in the test compound and 0.1 mol dm^{-3} in $[NBu_4][PF_6]$ as the supporting electrolyte. At the end of each voltammetric experiment, $[Fe(\eta^5\text{-}C_5H_5)_2]$ was added to the solution as an internal standard for potential measurements. Under the conditions used, the E^o value for the couple $[Fe(\eta^5\text{-}C_5H_5)_2]^+$–$[Fe(\eta^5\text{-}C_5H_5)_2]$ was 0.47 V.

Acknowledgments

This work was supported by the Spanish MEC (DGI)/FEDER (Projects CTQ2005-08606-C02-01, BFU2005-07422-C02-02, and MAT2005-1272) and the Gobierno de Aragón (Grupo de Excelencia: *Química Inorgánica y de los Compuestos Organometálicos*). We are indebted to Prof. Dr. S. Alvarez (Universitat de Barcelona) for kindly providing values of continuous shape measure.

Appendix A. Supplementary material

CCDC 629497 and 629498 contain the supplementary crystallographic data for this paper. These data can be obtained free of charge via http://www.ccdc.cam.ac.uk/conts/retrieving.html, or from the Cambridge Crystallographic Data Centre, 12 Union Road, Cambridge CB2 1EZ, UK; fax: (+44) 1223-336-033; or e-mail: deposit@ccdc.cam.ac.uk. Supplementary data associated with this article can be found, in the online version, at doi:10.1016/j.jorganchem.2007.03.028.

References

[1] M.J. Carney, in: R.H. Crabtree, D.M.P. Mingos (Eds.), in: K.H. Theopold (Ed.), Comprehensive Organometallic Chemistry III, vol. 5, Elsevier Ltd., Oxford, UK, 2007, pp. 291–390 (Chapter 5.05);
M.J. Morris, in: E.W. Abel, F.G.A. Stone, G. Wilkinson (Eds.), Comprehensive Organometallic Chemistry II, vol. 5, Elsevier Science, Ltd, Oxford, UK, 1995, pp. 471–549 (Chapter 8);

R. Davis, L.A.P. Kane-Maguire, in: G. Wilkinson, F.G.A. Stone, E.W. Abel (Eds.), Comprehensive Organometallic Chemistry, vol. 3, Pergamon Press, Oxford, UK, 1982, pp. 953–1077, Section 26.2.
[2] G.K. Barker, M.F. Lappert, J.A.K. Howard, J. Chem. Soc., Dalton Trans. (1978) 734;
G.K. Barker, M.F. Lappert, J. Organomet. Chem. 76 (1974) C45.
[3] (a) P.J. Alonso, J. Forniés, M.A. García-Monforte, A. Martín, B. Menjón, C. Rillo, Chem. Eur. J. 8 (2002) 4056;
(b) P.J. Alonso, L.R. Falvello, J. Forniés, M.A. García-Monforte, A. Martín, B. Menjón, G. Rodríguez, Chem. Commun. (1998) 1721.
[4] W. Seidel, G. Kreisel, Z. Anorg. Allg. Chem. 426 (1976) 150.
[5] F. Hein, D. Tille, Z. Anorg. Allg. Chem. 329 (1964) 72.
[6] F. Hein, K. Schmiedeknecht, J. Organomet. Chem. 5 (1966) 454.
[7] E. Müller, J. Krause, K. Schmiedeknecht, J. Organomet. Chem. 44 (1972) 127.
[8] P.J. Alonso, J. Forniés, M.A. García-Monforte, A. Martín, B. Menjón, Organometallics 24 (2005) 1269.
[9] J. Krausse, G. Marx, J. Organomet. Chem. 65 (1974) 215;
E. Kurras, J. Otto, J. Organomet. Chem. 4 (1965) 114.
[10] M.M. Olmstead, P.P. Power, S.C. Shoner, Organometallics 7 (1988) 1380;
F. Hein, R. Weiss, Z. Anorg. Allg. Chem. 295 (1958) 145.
[11] R. Poli, J. Organomet. Chem. 689 (2004) 4291;
R. Poli, Chem. Rev. 96 (1996) 2135.
[12] G.M. Barrow, S. Searles, J. Am. Chem. Soc. 75 (1953) 1175;
L.J. Bellamy, third ed.The Infra-Red Spectra of Complex Molecules, vol. 1, Chapman and Hall, Ltd, London, 1975, pp. 129–140 (Chapter 7).
[13] (a) A reduction of the $E_{1/2}$ potential was also observed in the $[V^{IV}R_4]/[V^{III}R_4]^-$ couple on decreasing the chlorination degree of the R group.;
(b) P.J. Alonso, J. Forniés, M.A. García-Monforte, A. Martín, B. Menjón, Chem. Eur. J. 11 (2005) 4713.
[14] W.N. Setzer, P. von Ragué Schleyer, Adv. Organomet. Chem. 24 (1985) 353.
[15] The continuous shape measure, S, gives a quantitative assessment on the extent to which the coordination environment of a real metal complex approaches a given ideal polyhedron. The smaller the value of S, the better the agreement between the real molecule and the suggested model, being $S = 0$ for perfect coincidence. For the definition of this structural parameter and its use in four- or six-coordinate complexes, see Ref. [16].
[16] (a) S. Alvarez, Dalton Trans. (2005) 2209;
(b) J. Cirera, P. Alemany, S. Alvarez, Chem. Eur. J. 10 (2004) 190;
(c) S. Alvarez, D. Avnir, M. Llunell, M. Pinsky, New J. Chem. 26 (2002) 996;
(d) M. Pinsky, D. Avnir, Inorg. Chem. 37 (1998) 5575.
[17] M. Llunell, D. Casanova, J. Cirera, J.M. Bofill, P. Alemany, S. Alvarez, M. Pinsky, D. Avnir, SHAPE (version 1.1), Universitat de Barcelona, The Hebrew University of Jerusalem, Spain, Israel.
[18] If the $Cr\cdots Cl^{ortho}$ interactions in complex **1** are disregarded, the remaining CrC_4 skeleton can alternatively be described as having a sawhorse arrangement—related to the so-called *Ψ-TBPY*-5 (see Ref. [16b]).
[19] C. Schulzke, D. Enright, H. Sugiyama, G. LeBlanc, S. Gambarotta, G.P.A. Yap, L.K. Thompson, D.R. Wilson, R. Duchateau, Organometallics 21 (2002) 3810.
[20] V. Gramlich, K. Pfefferkorn, J. Organomet. Chem. 61 (1973) 247.
[21] P. Stavropoulos, P.D. Savage, R.P. Tooze, G. Wilkinson, B. Hussain, M. Motevalli, M.B. Hursthouse, J. Chem. Soc., Dalton Trans. (1987) 557.
[22] C.J. Cardin, D.J. Cardin, J.M. Kelly, R.J. Norton, A. Roy, B.J. Hathaway, T.J. King, J. Chem. Soc., Dalton Trans. (1983) 671.
[23] I. Ara, J. Forniés, M.A. García-Monforte, A. Martín, B. Menjón, Chem. Eur. J. 10 (2004) 4186.
[24] P.J. Alonso, J. Forniés, M.A. García-Monforte, A. Martín, B. Menjón, Chem. Commun. (2002) 728, see also Ref. [23].
[25] P.J. Alonso, J. Forniés, M.A. García-Monforte, A. Martín, B. Menjón, Chem. Commun. (2001) 2138, see also Ref. [13].
[26] B.B. Garrett, M.T. Holbrook, J.A. Stanko, Inorg. Chem. 16 (1977) 1159;
M.T. Holbrook, B.B. Garrett, Inorg. Chem. 15 (1976) 150.
[27] F.J. Owens, in: F.J. Owens, C.P. Poole, H.A. Farah (Eds.), Magnetic Resonance of Phase Transitions, Academic Press, New York, 1979 (Chapter 6);
R. Alcalá, P.J. Alonso, R. Cases, J. Phys. C: Solid State Phys. 16 (1983) 4693.
[28] R.L. Carlin, Magnetochemistry, Springer-Verlag, Berlin, 1986, pp. 21–27, Section 2.3.
[29] Crystal data for **5′**: Monoclinic, space group $P2_1/n$, $a = 1466.4(1)$ pm, $b = 3092.2(1)$ pm, $c = 1468.2(1)$ pm, $\beta = 90.27(1)°$, $V = 6.659(1)$ nm^3; θ range for data collection: 2.07–24.97°; reflections collected: 12174; independent reflections: 11691 ($R_{int} = 0.0460$); final R indices [$I > 2\sigma(I)$]: $R_1 = 0.1026$, $wR_2 = 0.2993$; (all data) $R_1 = 0.1716$, $wR_2 = 0.3197$. All the atoms were refined anisotropically, but a large amount of unassigned electron density remained due to the poor quality of the crystal.
[30] J. Beck, M. Koch, Z. Anorg. Allg. Chem. 632 (2006) 756;
J. Beck, M. Koch, Z. Anorg. Allg. Chem. 630 (2004) 394;
J.C. Fettinger, S.P. Mattamana, R. Poli, Acta Crystallogr., Sect. C 54 (1998) 184;
J.C. Gordon, S.P. Mattamana, R. Poli, P.E. Fanwick, Polyhedron 14 (1995) 1339;
A.J. Blake, S. Parsons, A.J. Downs, C. Limberg, Acta Crystallogr., Sect. C 51 (1995) 571;
C.H. Schumacher, F. Weller, K. Dehnicke, Z. Anorg. Allg. Chem. 495 (1982) 135;
P. Klinzing, A. El-Kholi, U. Müller, K. Dehnicke, K. Findeisen, Z. Anorg. Allg. Chem. 569 (1989) 83;
C.D. Garner, L.H. Hill, F.E. Mabbs, D.L. McFadden, A.T. McPhail, J. Chem. Soc., Dalton Trans. (1977) 853.
[31] K.K. Sunil, M.T. Rogers, Inorg. Chem. 20 (1981) 3283.
[32] V.I. Murav'ev, Russ. J. Coord. Chem. 31 (2005) 837;
V.I. Murav'ev, Russ. J. Coord. Chem. 31 (2005) 609;
S. Patchkovskii, T. Ziegler, J. Chem. Phys. 111 (1999) 5730;
J. Swann, T.D. Westmoreland, Inorg. Chem. 36 (1997) 5348;
D.M. Sabel, A.A. Gewirth, Inorg. Chem. 33 (1994) 148;
K.K. Sunil, J.F. Harrison, M.T. Rogers, J. Chem. Phys. 76 (1982) 3087.
[33] W.A. Sheppard, J. Am. Chem. Soc. 92 (1970) 5419.
[34] P. Boudjouk, J.-H. So, in: R.N. Grimes (Ed.), Inorganic Syntheses, vol. 29, John Wiley & Sons, New York, 1992, pp. 108–111.
[35] C. Persson, C. Andersson, Inorg. Chim. Acta 203 (1993) 235.
[36] M.D. Rausch, F.E. Tibbetts, H.B. Gordon, J. Organomet. Chem. 5 (1966) 493.
[37] R. Usón, J. Forniés, Adv. Organomet. Chem. 28 (1988) 219–297;
E. Maslowsky Jr., Vibrational Spectra of Organometallic Compounds, John Wiley & Sons, New York, 1977, pp. 437–442.
[38] G.M. Sheldrick, SHELXL-97, Program for the Refinement of Crystal Structures from Diffraction Data, University of Göttingen, Göttingen, Germany, 1997.